Eur. Phys. J. D **44**, 109–116 (2007)
DOI: 10.1140/epjd/e2007-00150-5

THE EUROPEAN PHYSICAL JOURNAL D

Cubic and hexagonal symmetries in LiCl nanoclusters

P.C.R. Rodrigues and F.M.S. Silva Fernandes[a]

Department of Chemistry and Biochemistry, CCMM, Faculty of Sciences, University of Lisboa, Campo Grande, Bloco C8, 1749-016 Lisboa, Portugal

Received 19 September 2006 / Received in final form 23 February 2007
Published online 4 May 2007 – © EDP Sciences, Società Italiana di Fisica, Springer-Verlag 2007

Abstract. Cubic and hexagonal symmetries are observed in molecular dynamics simulations of lithium chloride unconstrained nanoclusters, using the Born-Mayer-Huggins (BMH) potential model. Phase changes between the two solid phases, and solid-liquid coexistences, are studied for LiCl clusters with a number of ions ranging from 1000 to 5292. A stability analysis of the clusters and bulk systems, at 0 K, is presented, using the BMH and the Michielsen-Woerlee-Graaf (MWG) potential models. The cubic structure from the BMH model is slightly more stable than the hexagonal one for cluster sizes between 1000 and ∼10 000 ions. For higher cluster sizes and bulk LiCl the opposite is true. Moreover, at 0 K, the bulk cubic phase from the MWG potential is significantly more stable than the hexagonal one. Thus, the BMH potential model seems unrealistic for large clusters and the bulk as far as a comparison with experiment is concerned. Finally, a fairly good correlation of the simulation results is obtained by means of a theoretical model recently reported by us.

PACS. 61.46.+w Nanoscale materials – 64.70.Nd Structural transitions in nanoscale materials – 64.70.Kb Solid-solid transitions

1 Introduction

Phase changes and phase coexistences in clusters have motivated a growing interest due to the theoretical challenges and the importance of their study in different fields, such as, nucleation, crystal growth, structure of amorphous materials, catalysis and atmospheric chemistry. The works on simple systems (like argon) [1–5], alkali halides [6–13], and metals [14–20], are just a few examples of the wide interest of this subject.

As an exact statistical mechanical theory to explain the behaviour of these systems constitutes a desirable but yet unattained objective, some approximated theoretical models have been proposed to correlate simulation and experimental data, and to predict new results [17,21–29].

Different solid phases in clusters have also been reported, for example, by Li and Huang [30] for iron and by Schebarchov and Hendy [31,32] for nickel and palladium. Moreover, experimental and theoretical works concerning solid(fcc)-solid(bcc) transitions in ionic salts under high pressure [33–35] have been presented, and Woodcock [36] has noted a solid(sc)-solid(bcc) transition for the bulk cesium chloride, whose energetics was studied by Pyper [37].

In the course of a previous work [38], the evolution of the temperature as a function of the total energy in clusters of lithium chloride, particularly for the 4096 ions size, suggested the possibility of different solid phases, although we have not developed the subject hitherto. The suggestion turned out by the observation of pronounced oscillations in the temperature through the phase coexistence regions.

The objective of the present work is to identify and characterise cubic and hexagonal symmetries in LiCl clusters by means of extensive MD simulations, and to analyse the results in the light of a theoretical model developed by us [29].

Recently, Croteau and Patey [39], motivated by the ab initio calculations of Aguado et al. [12], have reported the existence of cubic and ring-hexagonal solid symmetries in $(LiCl)_N$ clusters, with N ranging from 3 to 500, also using the BMH potential. Although the present study is based on a considerable higher number of ions and a more extensive analysis, some of our conclusions are in accordance with theirs.

The computational details are given in Section 2. Section 3 is devoted to the identification and characterisation of the different solid phases. Section 4 presents a further analysis of the simulation results. Section 5 contains the conclusions of this work and perspectives of future developments.

2 Computational details

Most of the molecular dynamics computations have been performed using the Born-Mayer-Huggins (BMH)

[a] e-mail: fsilva@fc.ul.pt

potential:

$$\phi_{ij}(r) = \frac{z_i z_j e^2}{r} + c_{ij} b \exp\left[\frac{\sigma_{ij} - r}{d}\right] - \frac{C_{ij}}{r^6} - \frac{D_{ij}}{r^8} \quad (1)$$

with the parameters given by Watts and McGee [40].

However, in order to analyse the relative stability of the clusters at 0 K we have also done some calculations with the Michielsen-Woerlee-Graaf (MWG) potential:

$$\phi_{ij}(r) = \frac{z_i z_j e^2}{r} + \frac{b}{r^l} \exp\left[k_{ij}(\sigma_{ij}^m - r^m)\right] - \frac{C_{ij}}{r^6} - \frac{D_{ij}}{r^8} \quad (2)$$

with the parameters given by Michielsen et al. [41] for $l = 4$ and $m = 1$.

It is well-known that these interaction models, despite being rigid-ion potentials, reproduce some bulk properties of alkali halides and other substances [42–48]. Recently, we have reported [49] an extensive study, by molecular dynamics and free energy calculations, of the phase diagrams for KCl and NaCl, using those models.

Verlet's leapfrog algorithm [50] for the numerical integration of Newton's equations of motion, with a time step of 5×10^{-15} s, has been used in all simulations. Thermal properties have been calculated with a number of steps in the range 10^5–10^8, depending on the size of the clusters and the phase transition region. Thus, the longer runs correspond to time scales of the order of 10^2 ns. The determination of the velocity auto-correlation functions has been based on runs of 1.6×10^4–4×10^6 time steps with a time origin at every fifth step.

As the clusters are unconstrained, the external pressure, p, is virtually zero. The calculation of each state point has been carried out by fixing the total energy, E, of the system and determining the corresponding average temperature, T (through the energy equipartition theorem [51]), instead of fixing a preset average temperature and calculating the resulting average total energy, as explained elsewhere [38,52]. The present calculations are, therefore, performed with the variables (n, p, E) fixed (n is the number of ions), not strictly in the context of the microcanonical ensemble (n, V, E) since the volume V is not constant. We should underline that there is nothing unusual in conducting constant-energy instead of constant-temperature simulations. Both approaches are able to detect phase transition regions in clusters. They also produce similar results for homogeneous phases. This is not so, however, specially at phase transition regions. In fact, it has been shown [21,22] that constant-energy and constant-temperature ensembles are not equivalent for finite systems such as nanoparticles. For example, a hallmark of constant-energy calculations is the negative values of the heat capacity at the coexistence regions, as seen in previous simulations [14,29,38,52] as well as in the present ones. Nonetheless, it turns out that constant--energy simulations are more suitable to assess some important aspects of phase changes in clusters, such as phase coexistences and their properties. The method of fixing the total energy of clusters was also used, for instance, by Briant and Burton [1], Cleveland et al. [23] and Nielsen et al. [14].

Table 1. Number of ions (n) and heating/cooling rates (10^9 kJ mol^{-1} s^{-1}): (a) initial simulations [38]; (b) current simulations.

n	(a)	(b)
1000	0.5	0.1
1728	3.7	0.5
2744	4.3	1.4
4096	4.3	1.4
5832	4.3	
8000	4.3	

The starting states for the heating processes have been f.c.c (rock salt) and hexagonal lattices at 0 K, with the appropriate number of ions for each kind of lattice. For the freezing, we have used two distinct starting points: (a) a totally melted configuration; (b) a configuration not completely melted containing residual crystallites [52].

Heating/cooling rates in the range 0.1–4.3 $\times$ 10^9 kJ mol^{-1} s^{-1} ($\sim 10^{10}$–10^{13} K s^{-1}) have been used. These rates were chosen in order to maintain the system as close to equilibrium as possible within the limits of computational expense.

3 Identification of the phases

Although our previous results for lithium chloride clusters [38] suggested the presence of more than one solid phase, they were insufficient for a thorough analysis mainly due to the high heating rates used. Therefore, we have performed improved simulations with lower heating/cooling rates (see Tab. 1). This is an essential detail since the appearance of the hexagonal phase is only occasional for the higher rates, becoming systematic for the lower ones.

The temperature as a function of total energy, for different cluster sizes, is represented in Figure 1, where the starting states for the heating curves have been cubic structures (cut from a perfect rock salt crystal). The heating curves starting from hexagonal structures shall be treated ahead.

The new results show well distinguishable "plateaus" connected by abrupt slopes. In order to confirm that, for a given cluster size, these features correspond to different phases, snapshots have been collected from each "plateau" in the neighbourhood of the slopes that connect them. Figure 2 displays snapshots for the 1728 ions cluster in convenient perspectives. In addition to the symmetry change, there are some other noticeable differences, such as: the liquid phase wets more extensively the hexagonal phase than the cubic one; the cubic structure appears in a distorted form that is wider near the liquid phase; the profile of the liquid wetting the cubic phase is similar to the one over a pair of contiguous faces in the hexagonal structure.

Figure 1 also shows some regular behaviours: (i) during heating, lithium chloride presents a double phase transition, cubic $\rightarrow$ cubic + liquid $\rightarrow$ hexagonal + liquid; (ii) spontaneous nucleation (see Ref. [52]) of the supercooled

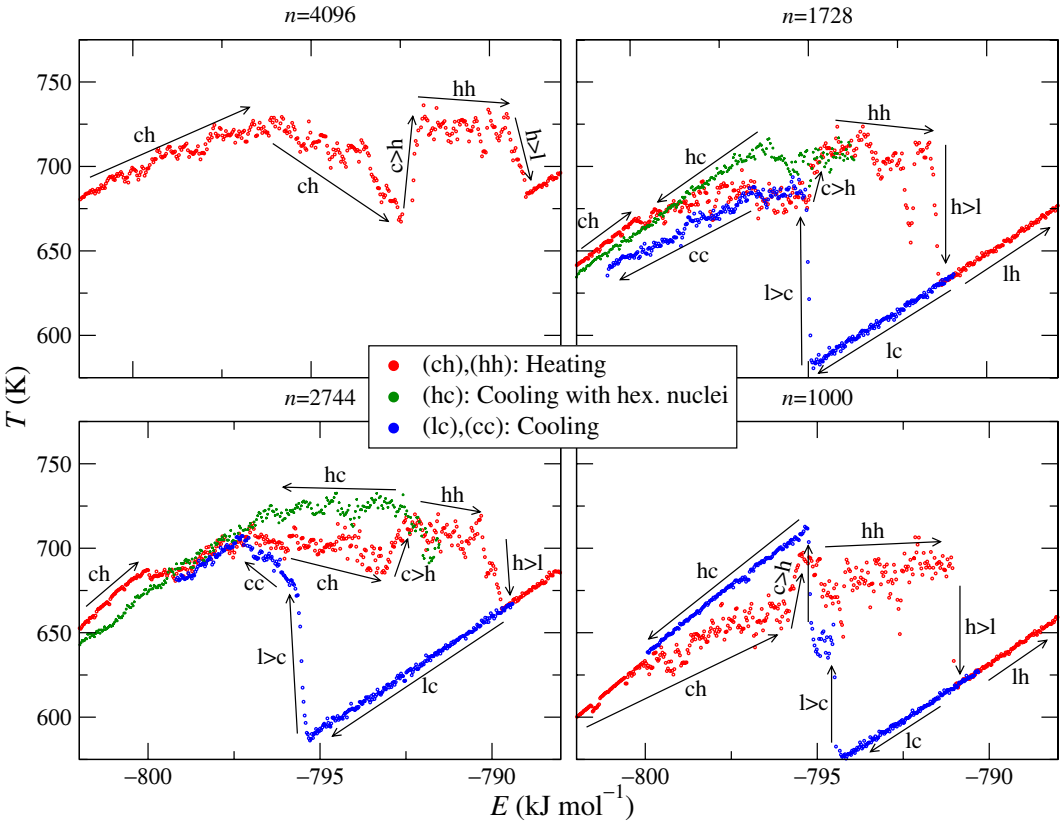

Fig. 1. (Color online) Temperature as a function of total energy for LiCl clusters of 1000, 1728, 2744 and 4096 ions, showing the occurrence of more than one solid phase. (ch) Cubic heating; (cc) cubic cooling; (hh) hexagonal heating; (hc) cooling with residual hexagonal nuclei; (lc) liquid cooling; (c > h) cubic to hexagonal; (h > l) hexagonal to liquid; (l < c) liquid to cubic. Arrows indicate the directions of the heating and cooling paths.

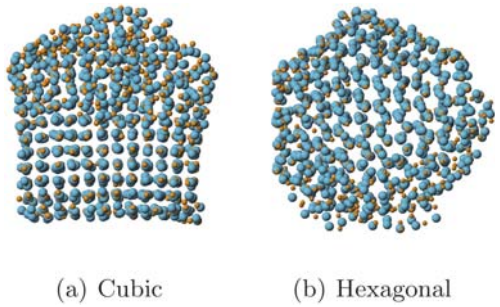

Fig. 2. Cubic and hexagonal symmetries in the 1728 ions cluster of LiCl during the melting starting from a cubic solid.

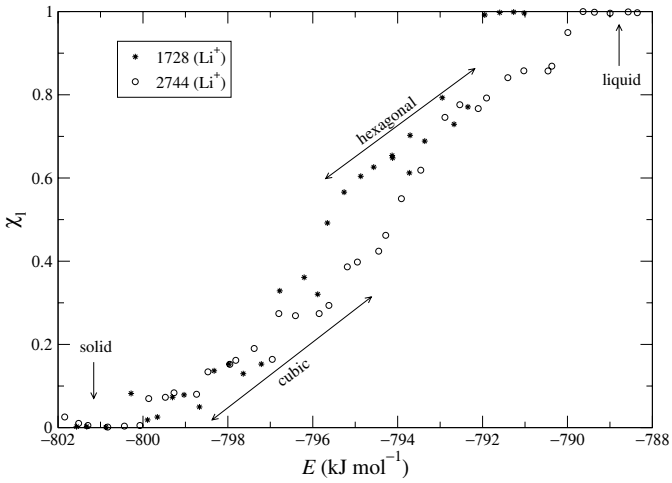

Fig. 3. Liquid molar fractions obtained during the melting of LiCl clusters with 1728 and 2744 ions.

liquid droplet occurs, always, with the formation of a cubic structure; and (iii) for the lower cooling rates, as in the 1000 ions cluster, a double transition, liquid → cubic + liquid → hexagonal + liquid, at fixed energy, is observed.

The last feature is consistent with the nucleation of the hexagonal phase in the liquid over the cubic phase, since no direct spontaneous liquid → hexagonal + liquid transition is observed. Thus, the cubic + liquid → hexagonal + liquid transition mechanism seems to have an intermediate step where the two solid phases coexist with the liquid. Then, due to the growth of the hexagonal phase, the temperature shall increase until the cubic phase is completely melted. However, since this is a relatively fast process, further refined calculations are needed to clarify such details.

The presence of the two phases can also be observed in the liquid molar fractions of Figure 3, obtained by means of the method based on the velocity autocorrelation functions reported elsewhere [38].

It is noteworthy that the general trends of the transitions from the cubic to hexagonal structures, in Figure 1, agree, qualitatively, with the entropy driven rearrangements claimed by Croteau and Pattey [39]. However, they do not report coexistent phases, certainly due to the small sizes of their clusters.

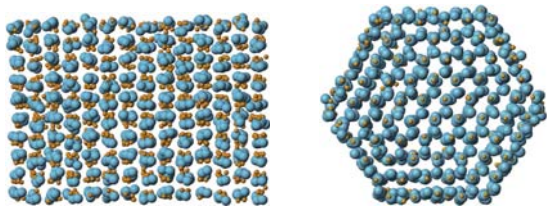

(a) Side view (b) Front view

Fig. 4. Hexagonal structure of a 2100 ions LiCl solid cluster at 600 K.

3.1 Hexagonal phase

To study the hexagonal phase, closed shell aggregates have been built and the minimum energy configurations determined. As an hexagonal structure have different symmetry elements, the relation between the number of concentric hexagonal shells and the number of planes is not trivial.

The number of particles for closed shells aggregates, like the one in Figure 4, is given by

$$n = np_{\mathrm{h}} \times 6 \times \sum_{i=1}^{nc_{\mathrm{h}}} (2i-1) \tag{3}$$

where np_{h} is the number of hexagonal planes and nc_{h} is the number of concentric shells of hexagons. That is

$$n = 6np_{\mathrm{h}} \left(nc_{\mathrm{h}}\right)^2. \tag{4}$$

The study made until now (for np_{h} between 1 and 20 and nc_{h} between 1 and 10) has allowed to identify the 1152, 2100, 3456, 5292 and 7680 cluster sizes as the lowest total energy configurations at 600 K. The minimum energy values suggest the rule:

$$np_{\mathrm{h}} = 2(nc_{\mathrm{h}} + 2) \tag{5}$$

whence

$$n = 12\left[\left(nc_{\mathrm{h}}\right)^3 + 2\left(nc_{\mathrm{h}}\right)^2\right]. \tag{6}$$

Figure 5 and Table 2 present the total energies of these hexagonal clusters and of cubic clusters in the same range of sizes. Since it is not possible, in general, to simultaneously build closed shell aggregates for the cubic and hexagonal structures with the same number of particles, an indirect comparison is made by representing the energy as a function of $n^{-1/3}$. The comparison suggests that for large clusters and bulk systems the hexagonal structures have slightly lower energies than the cubic ones, at 600 K. The free energies, at 0 K, represented in Figure 6 and Table 3, indicate that the hexagonal structure is slightly more stable than the cubic one for large clusters and bulk systems (the values of the bulk have been calculated using Ewald's sum for each solid symmetry). Since there is no experimental evidence of this behaviour, it appears that the BMH interaction model is unrealistic as far as large clusters of LiCl are concerned. We shall return to this problem ahead.

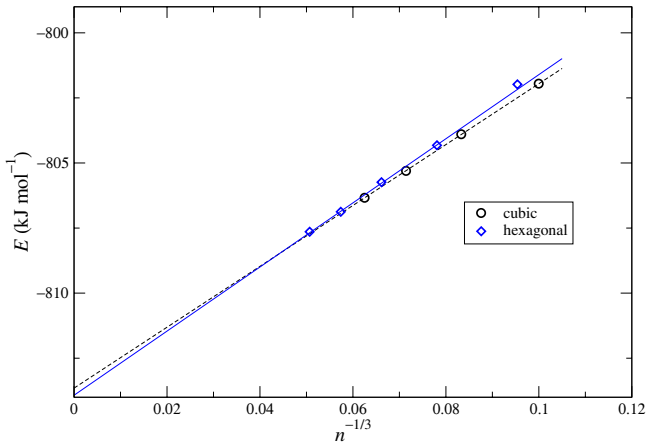

Fig. 5. Total energy, at 600 K, for LiCl aggregates (see Tab. 2). The lines are guides to the eye.

Table 2. Number of ions (n) and total energy (in kJ mol^{-1}) at 600 K for cubic and hexagonal LiCl clusters.

Cubic		Hexagonal	
n	E	n	E
1000	−801.958	1152	−801.980
1728	−803.896	2100	−804.320
2744	−805.304	3456	−805.740
4096	−806.338	5292	−806.876
		7680	−807.642

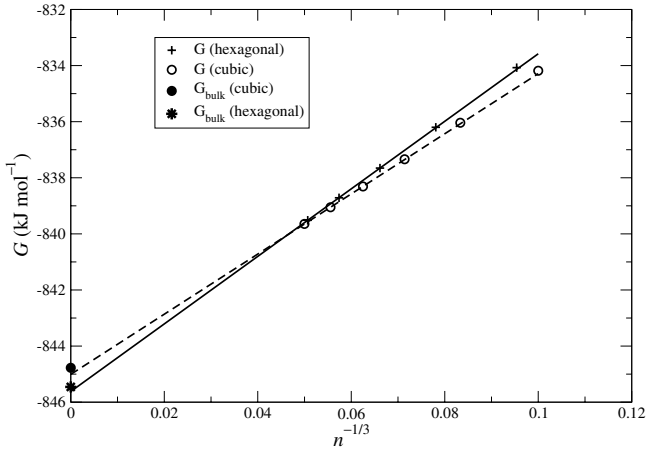

Fig. 6. Gibbs energies, at 0 K, for LiCl aggregates and the corresponding bulk systems (see Tab. 3). The lines are guides to the eye.

Table 3. Number of ions (n) and Gibbs energy (in kJ mol^{-1}), at 0 K, for LiCl aggregates and the corresponding bulk systems.

Cubic		Hexagonal	
n	E	n	E
1000	−834.186	1152	−834.074
1728	−836.042	2100	−836.200
2744	−837.342	3456	−837.654
4096	−838.308	5292	−838.714
5832	−839.052	7680	−839.514
8000	−839.648		
∞	−844.774	∞	−845.456

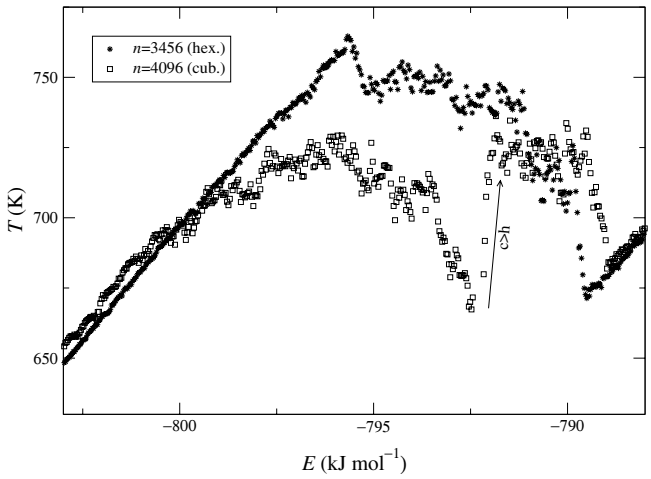

Fig. 7. Temperature as a function of energy for a (initially cubic) 4096 ions cluster and a (initially hexagonal) 3456 ions cluster of LiCl. The arrow indicates the transition from the cubic to hexagonal structures.

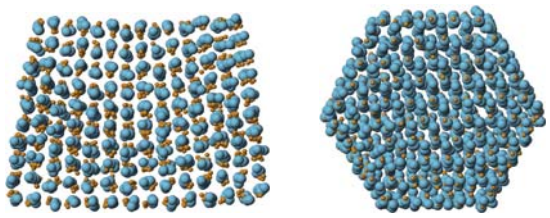

(a) Side view (b) Front view

Fig. 8. Asymmetric hexagonal variety of a 2100 ions LiCl cluster at 600 K.

Figure 7 displays the melting behaviours of a (initially cubic) cluster with 4096 ions and a (initially hexagonal) cluster with 3456 ions. The higher melting temperatures of the hexagonal clusters and the systematic transitions from cubic to hexagonal structures, but none from the hexagonal to the cubic ones, seem to confirm that the hexagonal symmetry is the more stable in this range of temperatures.

3.1.1 Hexagonal varieties

An asymmetric variety where the hexagonal planes are inclined (ones in relation to the others) appears in some circumstances during the simulations. Figure 8 shows views of this variety (see the symmetric structure in Figure 4 for comparison). This asymmetric variety is probably not compatible with macroscopic sizes considering the geometrical divergence of the hexagonal planes (see Fig. 8a). It also seems quite systematic below 600 K, but it is also observed, for example, at higher temperatures in the phase coexistence of the 1728 ions aggregate.

From the double transition liquid → cubic + liquid → hexagonal + liquid by slow freezing the 1000 ions cluster, it is possible to discern other variety. Figures 9a and 9b show that this new one also possesses the hexagonal symmetry axes but it is faceted in a different manner (see Figs. 9c and 9d).

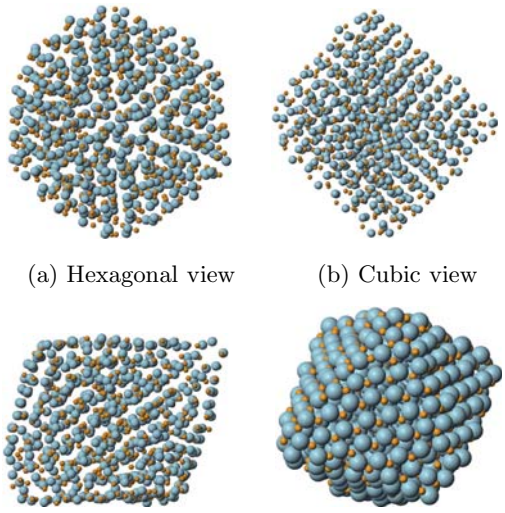

(a) Hexagonal view (b) Cubic view

(c) Tangent view (d) Volumic perspective

Fig. 9. Views of the structure formed during the freezing of a 1000 ions LiCl droplet.

4 Further analysis of the results

As two solid phases are observed, two kinds of critical nuclei should be involved, differing in geometry, and in internal and interfacial energies. The simulation results will now be analysed by means of a solid-liquid coexistence model reported elsewhere [29].

The key equation of the model is:

$$E = E_{\mathrm{l}(T_{\mathrm{m}})} + (T - T_{\mathrm{m}})C_p - k^3 \frac{\Delta h \; {T_{\mathrm{m}}}^3}{n(T_{\mathrm{m}} - T)^3} \qquad (7)$$

which assumes that phase coexistence is attained when the crystallite size becomes equal to the size of the critical nucleus. Indeed, at fixed total energy, the critical nucleus determines the state that maximises the entropy of the system [14,53].

In the last equation, k is given by:

$$k = \frac{4 \upsilon^{\frac{2}{3}} \sigma}{\Delta h} \qquad (8)$$

where υ is the specific volume of the solid, σ is the surface tension of the solid-liquid interface, and

$$E_{\mathrm{l}(T_{\mathrm{m}})} = E^{\infty}_{\mathrm{l}(T_{\mathrm{m}})} + \varsigma_{\mathrm{l}} n^{-\frac{1}{3}} \qquad (9)$$

$E_{\mathrm{l}(T_{\mathrm{m}})}$ is the total energy of the cluster at, or projected to, the bulk melting temperature, T_{m}. $E^{\infty}_{\mathrm{l}(T_{\mathrm{m}})}$ is the respective bulk limit energy, ς_{l} is the rate of change of the cluster total energy with system size, n, and

$$\Delta h = \Delta h^{\infty} + \Delta \varsigma n^{-\frac{1}{3}} \qquad (10)$$

Table 4. Enthalpy of melting (in $\mathrm{kJ\,mol^{-1}}$) and heat capacity (in $\mathrm{J\,K^{-1}mol^{-1}}$) for solid and liquid LiCl clusters at 650 K.

n	Geom	$C_p^{(s)}$	$C_p^{(l)}$	Δh
1000	fcc	58.80		9.884
1728	fcc	60.12	71.82	10.69
2100	hex	59.54		10.95
2744	fcc	60.12	71.26	11.27
3456	hex	59.90	70.72	11.53
4096	fcc		69.82	11.71
5292	hex	60.47		11.95
exp	–	61.70	65.02	19.83

Δh is the cluster enthalpy of melting, Δh^{∞} is the respective bulk limit, and $\Delta\varsigma$ is the rate of change of the melting enthalpy with system size. Solid-vapour and liquid-vapour interfacial energies are implicitly considered in equation (10) for the variation of the melting enthalpy with system size.

Considering the proximity of the energy values in the two solid phases (see Fig. 5), the same values of the parameters are used, for both phases, in equation (9). The heat capacities are nearly the same for the two solid structures (see Tab. 4). This is not so for the values of T_{m} and k^{∞} (the last is the limit of k when $n \to \infty$, and depends on υ and σ). That is to say, in the phase coexistence model context, the bulk melting temperatures, T_{m}, and k^{∞} are the essential parameters to distinguish the two phases.

Figure 10 contains the model predictions compared with the simulation results. $T_m = 850$ K and $k^{\infty} = 1.24$ for the hexagonal phase, and $T_m = 785$ K and $k^{\infty} = 1.00$ for the cubic phase. The values $E^{\infty}_{l(T_m)} = -797.61\ \mathrm{kJ\,mol^{-1}}$, $\Delta h^{\infty} = 14.74\ \mathrm{kJ\,mol^{-1}}$, $\varsigma_l = 67.376\ \mathrm{kJ\,mol^{-1}}$, $\Delta\varsigma = -48.564\ \mathrm{kJ\,mol^{-1}}$ and $C_p = 65\ \mathrm{J\,K^{-1}\,mol^{-1}}$ have been used for both structures.

If extremely low heating rates were used, a transition from the cubic to the hexagonal phase may be expected at the starting melting temperature and energy of the cubic structure. Nevertheless, due to the fact that closed shells correspond to different numbers of ions, in the two symmetries, and to the limitations of the model in the early stages of the melting, this prediction is presumably exact only for the infinite system. That is to say, a phase change from cubic to hexagonal structure is predicted for bulk LiCl at ∼785 K.

In Figure 1 three "plateaus" are distinguishable in the temperature evolution of initially cubic aggregates but, from the previous analysis, only two fit in the present model predictions and correspond to two distinct solid phases. The other one, at the very beginning of the melting region, seems to be related to a pre-early melting process of the cluster, even before the melting temperature predicted by the model is attained. Hexagonal aggregates with 2100 and 3456 ions show a small overheating relatively to that temperature, followed by a visible underheating (see Fig. 10). For the hexagonal 5292 ions aggregate pre-early melting also shows up similarly to the cubic phase.

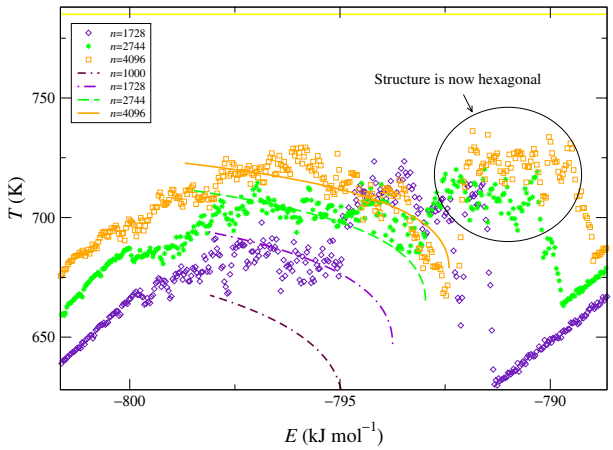

(a) Initially cubic

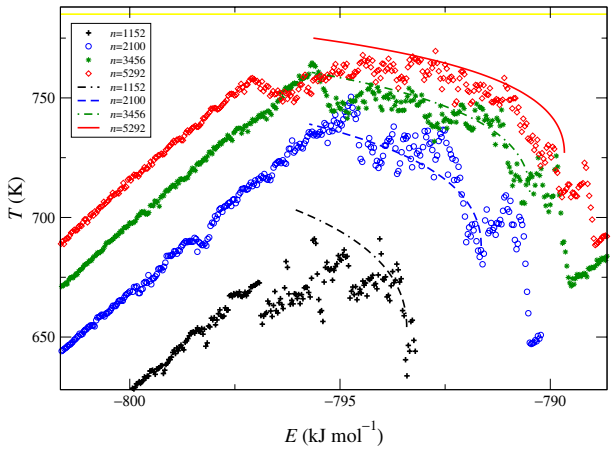

(a) Initially hexagonal

Fig. 10. (Color online) Model predicted temperature (lines) as a function of energy during the melting of initially cubic (1000, 1728, 2744 and 4096 ions) and initially hexagonal (1152, 2100, 3456 and 5292 ions) LiCl aggregates. Initially cubic 1000 ions simulation data is not represented for clarity.

The average temperatures, along the coexistence regions, show coarse periodicities, particularly for the smaller clusters. Although further and longer calculations are needed, most of these features are, presumably, a consequence of the short timescales probed being insufficient to cover the conformational rearrangements of the solid portions. Those features are, indeed, suggestive that establishment of ergodicity is very slow in this regime.

Like in the systems with a single solid phase, hysteresis cycles profiles are dependent on the heating/cooling rates. In the present study, though, a more diversified behaviour is observed due to the higher number of phases and the wider heating/cooling rate sensitivity. In the 1000 ions aggregate, for instance, a cycle with a path cubic → cubic + liquid → hexagonal + liquid → liquid during heating and liquid → cubic + liquid → hexagonal + liquid → hexagonal + glass during cooling is observed (see Fig. 1).

The simulation results based on the BMH potential, the stability analysis of Figures 5 and 6, and the model predictions, are consistent with the fact that the predicted

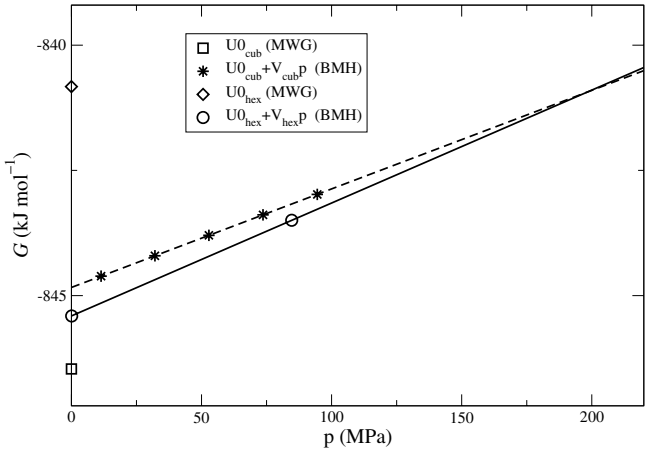

Fig. 11. Gibbs energy at 0 K as a function of pressure for bulk LiCl cubic and hexagonal structures.

bulk melting point of the hexagonal solid phase is nearer to the experimental value than the one predicted for the bulk cubic phase. Incidentally, preliminary calculations of the LiCl bulk phase diagram [54] with the same potential, also suggest a cubic-hexagonal transition and a higher melting point of the hexagonal phase.

We have questioned if the stability relation of the cubic and hexagonal structures can be inverted at non zero pressures. As can be seen in Figure 11, this inversion is only attained at ∼200 MPa (2000 bar) for bulk LiCl. Furthermore, the Gibbs energy at the same conditions using the MWG potential model (see Sect. 2) gives the cubic phase as significantly more stable (see Fig. 11 and Tab. 5) than the hexagonal one. This seems to confirm, as already referred to before, that the BMH model is unrealistic for bulk LiCl at low pressures, as far as a comparison with experiment is concerned.

Finally, in view of the present results for LiCl clusters using the BMH model, it appears that the ground states of the present cluster sizes have cubic symmetry (in accordance with the suggestion of Croteau and Patey [39] for clusters with more than 216 ions). Yet, this is not so for cluster sizes $\gtrsim$10 000 ions and the bulk, for which the ground states have a slightly more stable hexagonal symmetry.

5 Concluding remarks

The Born-Mayer-Huggins potential has been used to simulate lithium chloride nanoclusters. Two distinct solid structures, namely face centred cubic and hexagonal, have been detected with notorious differences on their melting behaviours.

A stability analysis of the clusters and bulk systems, at 0 K, has been presented, using the BMH and the MWG potential models. The cubic structure from the BMH model is slightly more stable than the hexagonal one for cluster sizes between 1000 and ∼10 000 ions. For higher cluster sizes and bulk LiCl the opposite is true. Moreover, at 0 K, the bulk cubic phase from the MWG potential is significantly more stable than the hexagonal one. Thus, the BMH potential model seems unrealistic for large clusters and the bulk as far as a comparison with experiment is concerned.

Table 5. Gibbs energy (in kJ mol^{-1}), at 0 K, as a function of pressure (in MPa) for cubic and hexagonal structures of bulk LiCl, from BMH and MWG potentials.

Cubic		Hexagonal	
p	G	p	G
(BMH potential)			
11.4040	−844.612	0.1346	−845.405
32.0908	−844.205	84.6591	−843.495
52.8358	−843.796		
73.6392	−843.388		
94.5010	−842.980		
(MWG potential)			
∼0	−846.464	∼0	−840.828

A fairly good correlation of the simulation results has been obtained by means of a theoretical model recently reported by us.

We hope that a further analysis of the lithium chloride melting and freezing, complemented by an extensive study of other salts, currently in progress, should improve the phase coexistence model. Additionally, the use of other potential models for lithium chloride is among the perspectives for future developments.

One of us (P. Rodrigues) gratefully acknowledges the institutional support of the Department of Chemistry and Biochemistry, FCUL, during his Ph.D. work. The authors thank Intel Corporation for the free access to their compilers and the GNU and Linux communities for all the invaluable tools they offer.

References

1. C.L. Briant, J.J. Burton, J. Chem. Phys. **63**, 2045 (1975)
2. N. Quirke, P. Sheng, Chem. Phys. Lett. **110**, 63 (1984)
3. J.E. Adams, R.M. Stratt, J. Chem. Phys. **93**, 1358 (1990)
4. D.J. Wales, R.S. Berry, J. Chem. Phys. **92**, 4295 (1990)
5. W. Polak, Eur. Phys. J. D **40**, 231 (2006)
6. M. Amini, D. Fincham, R.W. Hockney, J. Phys. C: Solid St. Phys. **12**, 4707 (1979)
7. M. Amini, D. Fincham, R.W. Hockney, J. Phys. C: Solid St. Phys. **13**, L221 (1980)
8. J.P. Rose, R.S. Berry, J. Chem. Phys. **96**, 517 (1992)
9. J.P. Rose, R.S. Berry, J. Chem. Phys. **98**, 3246 (1993)
10. J.P. Rose, R.S. Berry, J. Chem. Phys. **98**, 3262 (1993)
11. F.M.S.S. Fernandes, L.A.T.P. Neves, Am. Inst. Phys. Conf. Proc. **330**, 313 (1995)
12. A. Aguado, A. Ayuela, J.M. Lopez, J.A. Alonso, Phys. Rev. B **56**, 15353 (1997)
13. A. Aguado, L.E. González, J.M. López, J. Phys. Chem. B **108**, 11722 (2004)
14. O.H. Nielsen, J.P. Sethna, P. Stoltze, K.W. Jacobsen, J.K. Norskov, Eur. Phys. Lett. **26**, 557 (1994)
15. D.H.E. Gross, M.E. Madjet, Z. Phys. B **104**, 541 (1997)
16. C. Guet, X. Biquard, P. Blaise, S.A. Blundell, M. Gross, B.A. Huber, D. Jalabert, M. Maurel, L. Plagne, J.C. Rocco, Z. Phys. D **40**, (1997)

17. Y.G. Chushak, L.S. Bartell, J. Phys. Chem. B **105**, 11605 (2001)
18. S. Huang, P.B. Balbuena, J. Phys. Chem. B **106**, 7225 (2002)
19. L. Rangsu, L. Jiyong, D. Kejun, Z. Caixing, L. Hairong, Mater. Sci. Eng. B **94**, 141 (2002)
20. D. Schebarchov, S.C. Hendy, J. Chem. Phys. **123** (2005)
21. M. Bixon, J. Jortner, J. Chem. Phys. **91**, 1631 (1989)
22. D.J. Wales, R.S. Berry, Phys. Rev. Lett. **73**, 2875 (1994)
23. C.L. Cleveland, U. Landman, W.D. Luedtke, J. Phys. Chem. **98**, 6272 (1994)
24. D.H.E. Gross, E.V. Votyakov, Eur. Phys. J. B **15**, 115 (2000)
25. R.S. Berry, B.M. Smirnov, J. Chem. Phys. **114**, 6816 (2001)
26. D.H.E. Gross, Nuc. Phys. A **681**, 366C (2001)
27. O. Mulken, H. Stamerjohanns, P. Borrmann, Phys. Rev. E **64** (2001)
28. D.H.E. Gross, Phys. Chem. Chem. Phys. **4**, 863 (2002)
29. P.C.R. Rodrigues, F.M.S.S. Fernandes, Eur. Phys. J. D **41**, 113 (2007)
30. X. Li, J. Huang, J. Solid State Chem. **176**, 234 (2003)
31. D. Schebarchov, S.C. Hendy, Phys. Rev. Lett. **95** (2005)
32. D. Schebarchov, S.C. Hendy, Phys. Rev. B **73**, (2006)
33. Y. Sato-Sorensen, J. Geophys. Res. **88**, 3543 (1983)
34. N.V.K. Prabhakar, R.K. Singh, N.K. Gaur, N.N. Sharma, J. Phys. Cond. Mat. **2**, 3445 (1990)
35. H.R. Yazar, Turk J. Phys. **27**, 195 (2003)
36. L.V. Woodcock, *Corresponding states theory for the fusion of ionic crystals, in Proceedings of the Royal Society of London Series A-Mathematical Physical and Engeneering Sciences 348 (1653)* (1976), pp. 187–202
37. N.C. Pyper, J. Chem. Phys. **118**, 2308 (2003)
38. P.C.R. Rodrigues, F.M.S.S. Fernandes, Int. J. Quantum Chem. **84**, 169 (2001)
39. T. Croteau, G.N. Patey, J. Chem. Phys. **124**, 244506 (2006)
40. R.O. Watts, I.J. McGee, *Liquid State Chemical Physics* (John Wiley and Sons, 1976), pp. 307–312
41. J. Michielsen, P. Woerlee, F.V.D. Graaf, J.A.A. Ketelaar, J. Chem. Soc., Faraday Trans. II **71**, 1730 (1975)
42. L.V. Woodcock, Chem. Phys. Lett. **10**, 257 (1970)
43. L.V. Woodcock, K. Singer, Trans. Faraday Soc. **67**, 12 (1971)
44. M.J.L. Sangster, M. Dixon, Adv. Phys. **25**, 247 (1976)
45. F.J.A.L. Cruz, J.N.C. Lopes, J.C.G. Calado, M.E.M. da Piedade, J. Phys. Chem. B **109**, 24473 (2005)
46. F.J.A.L. Cruz, J.N.C. Lopes, J.C.G. Calado, J. Phys. Chem. B **110**, 4387 (2006)
47. N. Galamba, C.A.N. de Castro, J.F. Ely, J. Chem. Phys. B **108**, 3658 (2004)
48. N. Galamba, C.A.N. de Castro, J.F. Ely, J. Chem. Phys. **120**, 8676 (2004)
49. P.C.R. Rodrigues, F.M.S.S. Fernandes, J. Chem. Phys. **126**, 024503 (2007)
50. M.P. Allen, D.J. Tildesley, *Computer Simulation of Liquids* (Claredon Press, Oxford, UK, 1987)
51. K. Huang, *Statistical Mechanics* (John Wiley and Sons, New York, 1987)
52. P.C.R. Rodrigues, F.M.S.S. Fernandes, Eur. Phys. J. D **40**, 115 (2006)
53. M. Antoni, S. Ruffo, A. Torcini, Phys. Rev. E **66**, 025103(R) (2002)
54. P.C.R. Rodrigues, F.M.S.S. Fernandes, unpublished results (2006)